Clin Neuroradiol (2019) 29:231–242
https://doi.org/10.1007/s00062-018-0667-3

ORIGINAL ARTICLE

Diffusion Tensor Imaging of Dystrophic Skeletal Muscle

Comparison of Two Segmentation Methods Adapted to Chemical-shift-encoded Water-fat MRI

S. Keller[1] · Z. J. Wang[2] · A. Aigner[3] · A. C. Kim[4] · A. Golsari[5] · H. Kooijman[6] · G. Adam[1] · J. Yamamura[1]

Received: 4 September 2017 / Accepted: 12 January 2018 / Published online: 1 February 2018

Abstract

Purpose To compare the influence of two different regions of interest (ROIs) on diffusion tensor metrics in dystrophic thigh muscles using a custom-made (whole muscle) ROI including and a selective ROI excluding areas of fatty replacement.

Methods Diffusion tensor imaging (DTI) and chemical-shift-encoded water-fat magnetic resonance imaging (MRI) of the thigh was conducted on a 3-Tesla system in 15 cases with muscular dystrophy and controls. The ROIs were chosen according to patterns of fatty replacement on co-registered axial DTI and gradient echo sequence (GRE) images. Fractional anisotropy (FA), apparent diffusion coefficient (ADC), fiber track length (FTL), and muscle fat fractions (MFF) were compared between both ROI segmentations. These comparisons, muscle-specific correlation coefficients, and the influence of ROI localization on tensor metrics were derived based on linear mixed effects regression models.

Results In the cases a high correlation was observed for ADC and FA with MFF using a custom ROI. The correlation was weaker but still significant with a selective ROI method. Using the custom ROI, FTL correlated significantly with MFF in 3 out of 4 muscles ($r \leq -0.51$). A correlation was not found for the selective ROI method. Interaction analysis revealed that the association of ADC and FA with MFF was not significantly influenced by the ROI localization. For FTL the ROI localization significantly reduced the negative association with MFF.

Conclusion The DTI metrics and FTL of custom ROI segmentation are significantly influenced by MFF. Contrary to ADC and FA, the effect of MFF on FTL is significantly reduced when applying selective ROI segmentation, which could therefore be a better option for MR tractography.

Keywords Magnetic resonance imaging · Diffusion tractography · Muscular diseases · Fractional anisotropy · Apparent diffusion coefficient

Abbreviations

ADC	Apparent diffusion coefficient
BF	Biceps femoris muscle
DTI	Diffusion tensor imaging
EPI	Echo planar imaging
FA	Fractional anisotropy
FTL	Fiber track length
G	Gracilis muscle
GRE	Gradient echo sequence
MFF	Muscle fat fraction
NSA	Number of signal averages
RF	Rectus femoris muscle
ROI	Region of interest
SNR	Signal-to-noise ratio
ST	Semitendinosus muscle

Electronic supplementary material The online version of this article (https://doi.org/10.1007/s00062-018-0667-3) contains supplementary material, which is available to authorized users.

✉ S. Keller
s.keller@uke.de

Extended author information available on the last page of the article

Introduction

The human skeletal muscle is a highly organized organ consisting of muscle fascicles, subdivided into contractile units of myofibrils containing myosin and actin [1]. The connective tissue that surrounds and covers each muscle fiber (endomysium) and fascicle (perimysium) forms the basis for internal architecture, fiber architecture and orientation being highly predictive of functional capacity [2,

3]. Pathophysiological changes of the skeletal muscle often start at the cellular or fascicular level, beyond the detection capability of regular T1- and T2-weighted magnetic resonance imaging (MRI) [4]. Diffusion tensor imaging (DTI) has been promoted as a sensitive and non-invasive tool for detection and assessment of these subtle processes caused by trauma, inflammation or dystrophic processes, reflected by alterations in tissue diffusivity [5–11]. Beyond that, DTI enables visualization of muscle architecture by combining the principal diffusion directions of neighboring voxels for 3D fiber tractography [12, 13].

The application of DTI for dystrophic skeletal muscle is challenging, as a high signal-to-noise is needed to obtain accurate estimates of DTI metrics. Previous studies demonstrated that the reliability of estimated DTI parameters is affected by the percentage of fat in muscle, higher percentages resulting in overestimation of fractional anisotropy (FA) and underestimation of the apparent diffusion coefficient (ADC) [14–16]. It remains a matter of debate whether these effects should be regarded as confounding factors or as potential biomarkers, for example, for a Duchenne muscular dystrophy patient cohort as previously proposed by Ponrartana et al. [9].

An easily and readily applicable technique in routine clinical MRI is the quantitative evaluation of muscular fatty replacement using chemical-shift-encoded water-fat separation MRI [17, 18]. In contrast to neurological causes of muscular atrophy (e. g. denervation processes), the fat infiltration in muscular dystrophy is non-uniformly distributed within a single muscle [19] sometimes targeting certain muscle groups, which can be used to narrow down the differential diagnosis [20].

The aim of this study was to compare the influence of two different region of interest (ROI) selections on muscle fat, DTI metrics, and fiber track length (FTL) in the thigh muscles of patients with muscular fatty replacement due to dystrophic and myopathic conditions using

a) a whole muscle custom-made ROI including, and
b) a selective ROI excluding, areas of fatty replacement on geometrically co-registered axial DTI and gradient echo sequence (GRE) images.

Methods

Study Population

Data for this study were prospectively collected between May 2014 and March 2017. The study was approved by

Table 1 Diagnosis and demographics including muscle fat fraction and presence of muscle edema in the cases studied

Diagnosis	Genetics	Gender	Age (years)	BMI (kg/m^2)	CK (U/l)	MFF median (range) (%)	Muscle edema
Facioscapulohumeral muscular dystrophy	*D4Z4 repeat, 4q35*	M	68	28.3	437	5.7 (4.6–7.8)	VL
Facioscapulohumeral muscular dystrophy	*D4Z4 repeat, 4q35*	F	49	28.3	417	53.4 (40.5–82.8)	–
Limb girdle muscular dystrophy 2A	*CAPN 3, 15q15.1*	F	66	27.0	289	32.7 (7.4–70.6)	–
Limb girdle muscular dystrophy 2A	*CAPN 3, 15q15.1*	M	26	29.3	276	77.3 (71.5–81.7)	–
Limb girdle muscular dystrophy unknown	n. d.	F	52	25.1	800	42.2 (8.0–71.9)	–
Becker muscular dystrophy	*DMD, Xp21.2*	M	34	30.5	830	5.8 (2.9–9.7)	VM
Becker muscular dystrophy	*DMD, Xp21.2*	M	31	17.5	1820	31.9 (7.9–63.5)	VL, ADM
Duchenne muscular dystrophy	*Xp21.2-p21.1*	M	22	20.9	690	89.8 (85.0–91.8)	–
Myotonic dystrophy 1	*DMPK, 19q13.3*	F	25	18.5	401	5.2 (3.7–6.2)	–
Myotonic dystrophy 1	*DMPK, 19q13.3*	M	36	28.7	431	5.5 (2.7–8.4)	VM, ADM
Myotonic dystrophy 2	*ZNF9, 3q21.3*	M	74	23.7	96	8.9 (7.5–10.9)	VM, ADM
Spinal muscular atrophy type 3	*SMN1, 5q13.2*	F	51	22.2	n. d.	20.2 (6.2–37.2)	VI
Spinal muscular atrophy type 3	*SMN1, 5q13.2*	M	21	22.1	n. d.	6.3 (3.9–9.6)	–
Central core disease	*RYR1, 19q13.2*	M	56	22.1	526	13.3 (10.5–20.2)	VM
Immune mediated necrotizing myopathy	*Sporadic*	F	72	22.0	674	10.8 (6.5–17.6)	VL

BMI body mass index, *CK* creatine kinase, *MFF* muscle fat fraction, *VL* vastus lateralis muscle, *VM* vastus medialis muscle, *ADM* adductor magnus muscle, *VI* vastus intermedius muscle

Table 2 Sequence parameters for T2-weighted, gradient echo sequence, and diffusion tensor imaging sequence

Sequence	Plane	Slice thickness (mm)	FOV	Voxel size (mm^3)	Reconstruction pixel size (mm)	Acquisition matrix	Flip angle (°)	TR (ms)	TE (ΔTE) (ms)	b-value (s/mm^2)	Number of gradient directions	Number of signal averaging
T2 Dixon	Axial	3	270 × 221 × 300	0.65 × 0.65 × 3.0	0.469	416 × 342	90	8111	80	N/A	N/A	N/A
GRE Dixon	Axial	1	250 × 250 × 250	1.0 × 0.5 × 2.0	0.488	124 × 249	3	4.2	1.19 (2.5)	N/A	N/A	N/A
DTI	Axial	6	220 × 220 × 240	1.5 × 1.5 × 4.0	0.98	148 × 145	90	2479	66	0, 500	15	8

GRE gradient echo sequence, *DTI* diffusion tensor imaging, *FOV* field of view, *TR* repetition time, *TE* echo time, *N/A* not applicable

the institutional review board (PV4750) and written informed consent was obtained from each patient and control prior to MRI. The study cohort consisted of 15 cases (45.7 ± 19.3 years; male:female 9:6) with diagnosed muscular dystrophy or myopathy and 11 healthy controls (46.4 ± 14.1 years; male:female 6:5). Demographic details of the cases are included in Table 1. Absence of the use of medication altering skeletal muscle metabolism, recent trauma, or discomfort of the proximal limb muscles were prerequisites.

MRI Procedure

All MRI scans of the thigh were performed on a 3.0-Tesla (T) MRI system (Ingenia, Software Release 5.1.7, Philips, Best, The Netherlands). Subjects were examined in a supine position, feet first, using a 28-channel sensitivity encoding torso array coil. The total duration of the scan was approximately 45 min and contained:

(i) Axial T2-weighted turbo spin echo sequence with modified Dixon fat-water separation [21] (T2w mDixon).
(ii) Axial 3D GRE modified Dixon sequence. Post-processing produced in-phase and opposed-phase based water and fat-only images.
(iii) DTI using an axial fat-suppressed multislice single-shot spin-echo echo planar imaging (SS SE-EPI) sequence covering the same anatomic volume of both GRE and T2w scans. Details of sequences used are depicted in Table 2.

Image Analysis

Quantitative DTI analysis was performed using an offline workstation and software (FiberTrak; release V2.1.3 Philips Healthcare, Cleveland, OH). Geometrically co-registered axial DTI and GRE images were used to identify different muscles and to visualize areas of fatty replacement within the muscle. For the study three ROIs were drawn by two operators by consensus (4 years and 12 years of experience in MRI, respectively) using two different approaches of ROI localization:

a) a *custom ROI* covering the whole muscle and
b) *selective ROI* excluding areas of fatty infiltration.

The ROIs were chosen for the rectus femoris (RF), semitendinosus (ST), biceps femoris (BF), and gracilis (G) muscles. Fig. 1 gives an overview of the muscles analyzed. In both techniques diffusion images were registered to the b = 0 image prior to performing fiber tracking. For fiber tracking, the software employed a fiber assignment by continuous tracking (FACT) method using thresholds previously defined by Mori et al. [22, 23]. Quantitative pixel-

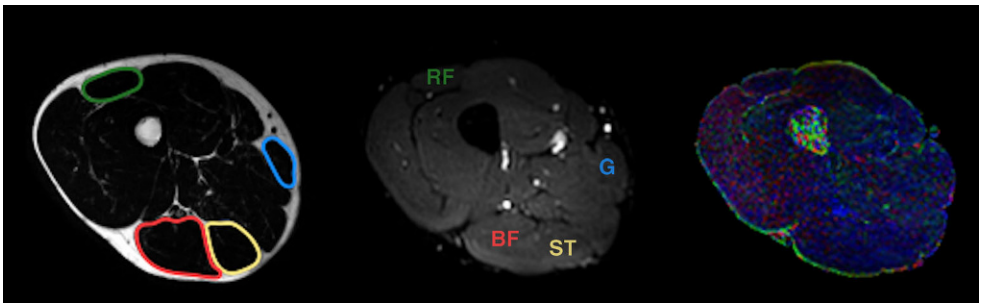

Fig. 1 Muscles chosen for diffusion tensor analysis. Axial GRE imaging, axial DTI (b = 0 s/mm^2), and colored FA map (*left to right*) (*RF* rectus femoris, *ST* semitendinosus, *BF* biceps femoris, *G* gracilis muscle)

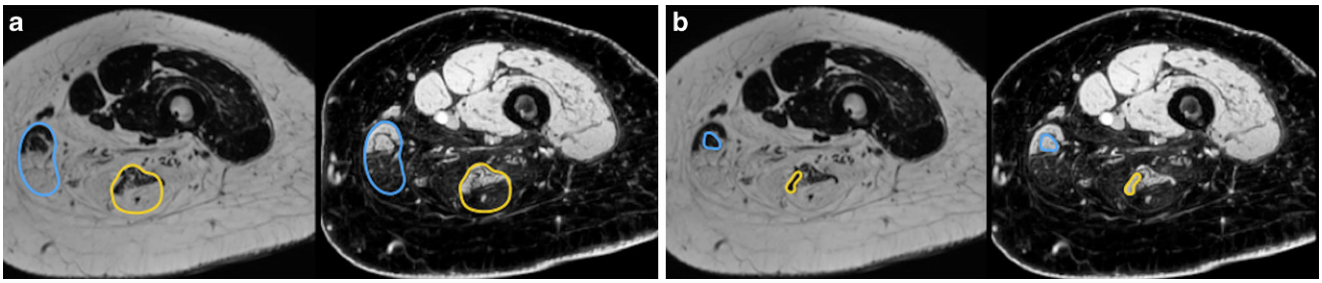

Fig. 2 Illustration of custom and selective ROI localization on GRE fat only (*left*) and water only (*right*) axial image of a 52-year-old female with diagnosed limb girdle muscular dystrophy, **a** whole muscle custom ROI, **b** selective ROI excluding areas of fatty replacement (*yellow circle* semitendinosus muscle, *blue circle* gracilis muscle)

based data (FTL, FA and ADC) were calculated automatically from measurements along the reconstructed fiber track by the software using a single pixel-based line propagation technique with a FTL threshold of 10 mm, a FA threshold of 0.1, and a direction threshold of 27° to minimize the effect of noise on fiber track reconstruction. The algorithm also accounts for noise caused by signal loss from using a fat-suppressed echo planar imaging sequence on predominantly fat-replaced tissue, as this could be the case in dystrophic skeletal muscle.

Muscle Tissue Custom Approach

In the custom approach, three ROIs (mean size 509.7 ± 19.4 mm^2) encircling the inner border of the transverse cross-sectional area of each muscle bundle were chosen by using the axial co-registered DTI and GRE images provided by the manufacturer's software (Fig. 2a).

Muscle Tissue Selective Approach

Small ROIs of varying size (mean 68.1 ± 8.7 mm^2) were carefully chosen for the remaining muscle tissue within the degenerative muscle bundle, avoiding areas of fatty tissue (Fig. 2b). Due to the lack of areas of remaining muscle tissue on axial T1w images, two cases had to be excluded from the selective ROI method. Given that healthy skeletal muscle is not infiltrated by fatty tissue, selective ROI localization was not performed in controls.

Muscle Fat Fraction

The muscle fat fraction (MFF) was obtained using axial 3D GRE modified Dixon sequence with chemical-shift-encoded reconstruction of the fat and water signal [18, 24]. A bias caused by the different T1 values of fat (around 450 ms) and muscle (around 1350 ms), was minimized by a small pulse angle of 3° chosen for the Dixon GRE sequence. Using the signal formula for spoiled gradient echo sequences, the residual T1 weighting causes an overestimation of fat signal by around 27%, which was corrected for when calculating the fat fraction. A T2* correction is incorporated in the Dixon algorithm of the system software [21].

A custom imaging software (OsiriX; version 6.5; Pixmeo, Bernex, Switzerland) was used to derive the signal intensity (SI) of three ROIs. ROIs were drawn on the reconstructed fat and water-only image of the proximal, middle, and distal muscle samples according to the ROI localization chosen for the custom and selective DTI analyses. Quantitative MFF were calculated as $[SI_{FAT}/(SI_{FAT}+SI_{WATER})]\times 100$ and reported as mean value of all pixels within a ROI.

Statistical Analysis

Due to the clustered data structure (clustering within patients and muscles), classical linear regression models which assume independency of observations cannot be used. Therefore, Pearson correlations were selectively applied on all individual muscles. Differences in custom DTI

metrics (FA, ADC) and FTL between cases and controls and between the custom and selective ROI method were visualized with boxplots and tested using linear mixed effects regression models with random intercepts for muscle and patient. These models take the dependencies in the data into account, and regression coefficients other than the intercept can be interpreted as usual. These models were also used to test the differences in the effect of MFF on selective cases and custom cases DTI metrics and FTL. Due to the explorative nature of our analyses we did not adjust for multiple testing. Significant results therefore have to be interpreted with care. A P-value <0.05 was considered statistically significant. For all analyses the statistical software R [25] was used, the ggplot2 [26] package for visualization, and the lme4 [27] package for mixed effects models.

Results

Imaging Findings

In the healthy controls, GRE and T2w mDixon imaging depicted normal shape and symmetry of the thigh muscles with a dense distribution of myofibrils within the different muscle groups, without signs of intramuscular edema or fatty infiltration.

In cases, signs of muscular atrophy with varying degrees of fatty replacement were visible on the initial GRE images. The grade of muscular degeneration and fatty infiltration followed a disease-specific pattern, for example, with a ragged reticular pattern in spinal muscular atrophy type 3 [28] and a hourglass pattern with predominantly very high or very low and discontinuous fatty replacement in facioscapulohumeral muscular dystrophy (Fig. 3; [29, 30]).

Muscle Fat Fraction Derived from Custom and Selective ROI Segmentation in Cases and Controls

In controls, the average MFF for all thigh muscles (RF, ST, BF, G, $N=44$) was 4.7 ± 2.2% (range: 1.2–9.7%). Using custom ROI analysis in cases, the mean MFF ($N=60$) was significantly increased (27.3 ± 2.9%; range: 2.7–91.8%; $P<0.001$). On selective ROI segmentation the mean MFF ($N=52$) was 4.9 ± 3.7% (range 1.2–15.5%) which differed significantly from MFF using the custom ROI analysis ($P<0.001$). Table 3 summarizes the muscle-specific mean DTI metrics, FTL and MFF of cases and controls.

Differences Between DTI Metrics and FTL of Custom and Selective ROI Localization in Cases and Controls

The mean ± SD ADC in controls was 1.63 ± 0.20 $mm^2/s \times 10^{-3}$ and corresponded to a mean ± SD FA of 0.31 ± 0.06. The mean ± SD FTL in controls was 57.5 ± 27.2 mm. For visualization of muscle fibers, Fig. 4a–c shows the grey scale FA maps and 3D tractography of a healthy control and two cases with mild to severe loss of muscle tissue and fatty replacement.

Using custom ROI segmentation in cases, the mean ± SD ADC and FTL were significantly lower with 1.28 ± 0.45 $mm^2/s \times 10^{-3}$ ($P<0.001$) and 43.4 ± 24.1 mm ($P<0.001$), respectively. These findings corresponded to a significantly increased mean ± SD FA of 0.46 ± 0.14 ($P<0.001$).

The mean ± SD ADC of the selective ROI segmentation in cases was 1.59 ± 0.26 $mm^2/s \times 10^{-3}$. The mean ± SD FA and FTL were 0.37 ± 0.09 and 47.5 ± 24.4 mm, respectively. No significant difference was observed between selective ROI segmentation-derived DTI metrics and FTL in cases compared to controls. Muscle-specific DTI metrics, FTL and MFF for both segmentation methods as well as controls are summarized in Table 3. In neither cases nor controls, associations between age or body mass index (BMI) and DTI metrics, FTL, or MFF were detected (Supplementary Table 1).

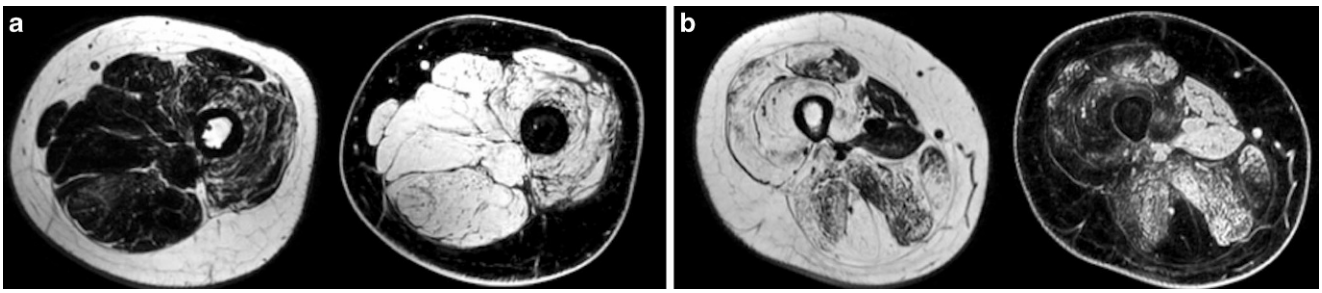

Fig. 3 A 21-year-old male with diagnosed spinal muscular atrophy type 3 (**a**) and a 49-year-old female with diagnosed facioscapulohumeral muscular dystrophy (**b**). Disease-specific pattern of fatty distribution with a ragged reticular patter (**a**) and a hourglass and discontinuous (**b**) distribution in the respective disease. Axial GRE fat-only (*left*) and water-only (*right*) images

Table 3 Mean MFF%, DTI metrics and FTL of custom and selective region-of-interest localization in cases and controls

Muscle ID		Mean (standard deviation)			
Cases					
–	Region of interest (ROI)	MFF (%)	FA	ADC ($mm^2/s \times 10^{-3}$)	FTL (mm)
RF	Custom	19.9 (27.7)	0.42 (0.16)	1.48 (0.49)	39.5 (18.6)
	Selective	2.8 (1.5)	0.34 (0.09)	1.74 (0.32)	44.1 (26.5)
ST	Custom	33.8 (32.5)	0.45 (0.14)	1.25 (0.43)	57.1 (32.1)
	Selective	5.2 (3.8)	0.36 (0.09)	1.55 (0.22)	57.3 (29.9)
G	Custom	22.2 (27.1)	0.53 (0.11)	1.16 (0.36)	43.5 (20.8)
	Selective	4.6 (2.5)	0.43 (0.08)	1.49 (0.18)	51.8 (22.4)
BF	Custom	33.2 (30.5)	0.45 (0.15)	1.24 (0.42)	33.5 (15.2)
	Selective	7.1 (5.0)	0.35 (0.07)	1.57 (0.22)	36.9 (17.8)
Controls					
RF		2.4 (1.0)	0.27 (0.05)	1.84 (0.21)	42.1 (25.8)
ST		5.3 (2.3)	0.30 (0.04)	1.60 (0.13)	77.6 (25.6)
G		4.8 (1.6)	0.39 (0.05)	1.49 (0.11)	66.8 (22.5)
BF		6.1 (1.7)	0.28 (0.04)	1.59 (0.13)	43.6 (14.3)

Custom ROI cases, $N = 60$
Custom ROI controls, $N = 44$
Selective ROI cases, $N = 52$
MFF muscle fat fraction, *ADC* apparent diffusion coefficient, *FA* fractional anisotropy, *FTL* fiber track length, *RF* rectus femoris, *ST* semitendinosus, *BF* biceps femoris, *G* gracilis

Comparison of Custom and Selective ROI Segmentation in Cases

By applying selective ROI segmentation, the data structure showed lesser variability as expressed by a lower standard deviation within the three technical replicate ROIs chosen for each muscle (Supplementary Table 2). Using linear mixed effects regression models with random intercepts for muscle and patient, the mean MFF and FA differed significantly between custom and selective ROI segmentation ($P < 0.001$), but not ADC and FTL (Fig. 5).

Correlation of Custom and Selective ROI Analysis in Cases

The FA obtained in both segmentation methods correlated strongly in cases (r = 0.81, 95% CI 0.69; 0.89). A significant correlation was also observed for ADC and FTL in cases (r = 0.49, 95% CI 0.24; 0.67; r = 0.76, 95% CI 0.62; 0.86, respectively) (Supplementary Table 3).

Differences Between Custom and Selective ROI Segmentation in Correlation of DTI Metrics and FTL with MFF

Table 4 summarizes the Pearson correlation coefficient and confidence intervals for each muscle analyzed and each segmentation method applied. A consistent and strong correlation of ADC and FA with MFF was observed in each muscle of cases when using custom ROI segmentation (r = –0.85 to –0.91 and r = 0.83–0.93, respectively). By applying the custom ROI, FTL significantly correlated to MFF in ST, G and BF muscle (r = –0.51 to –0.83), but not RF muscle (r = –0.31).

The association of ADC and FA with MFF on custom ROI was weaker but still significant when using the selective ROI in ST, G, and BF muscles, but not RF muscle (r = –0.65 to –0.76 and r = 0.57–0.72, respectively). For FTL, the significant association with MFF on custom ROI was removed by applying the selective ROI in G and BF muscle (r = –0.32 to –0.33) and remained at a lower degree in ST muscle (r = –0.58). No significant correlation of DTI metrics and FTL was found when correlation analysis was applied for each separate muscle in controls.

Effect of Selective ROI Segmentation on Association of MFF with DTI Metrics and FTL in Cases

The Pearson correlation coefficients between MFF on the one hand, and DTI metrics and FTL on the other hand, differed between custom and selective ROI, irrespective of being significantly different from zero. This may indicate that the effect of MFF depends on whether custom or selective areas are investigated, a finding that can only be tested in a regression model including all measurements and the interaction term between MFF and the ROI placement. The results of these models revealed that the effect of MFF on ADC and FA was not significantly influenced by ROI local-

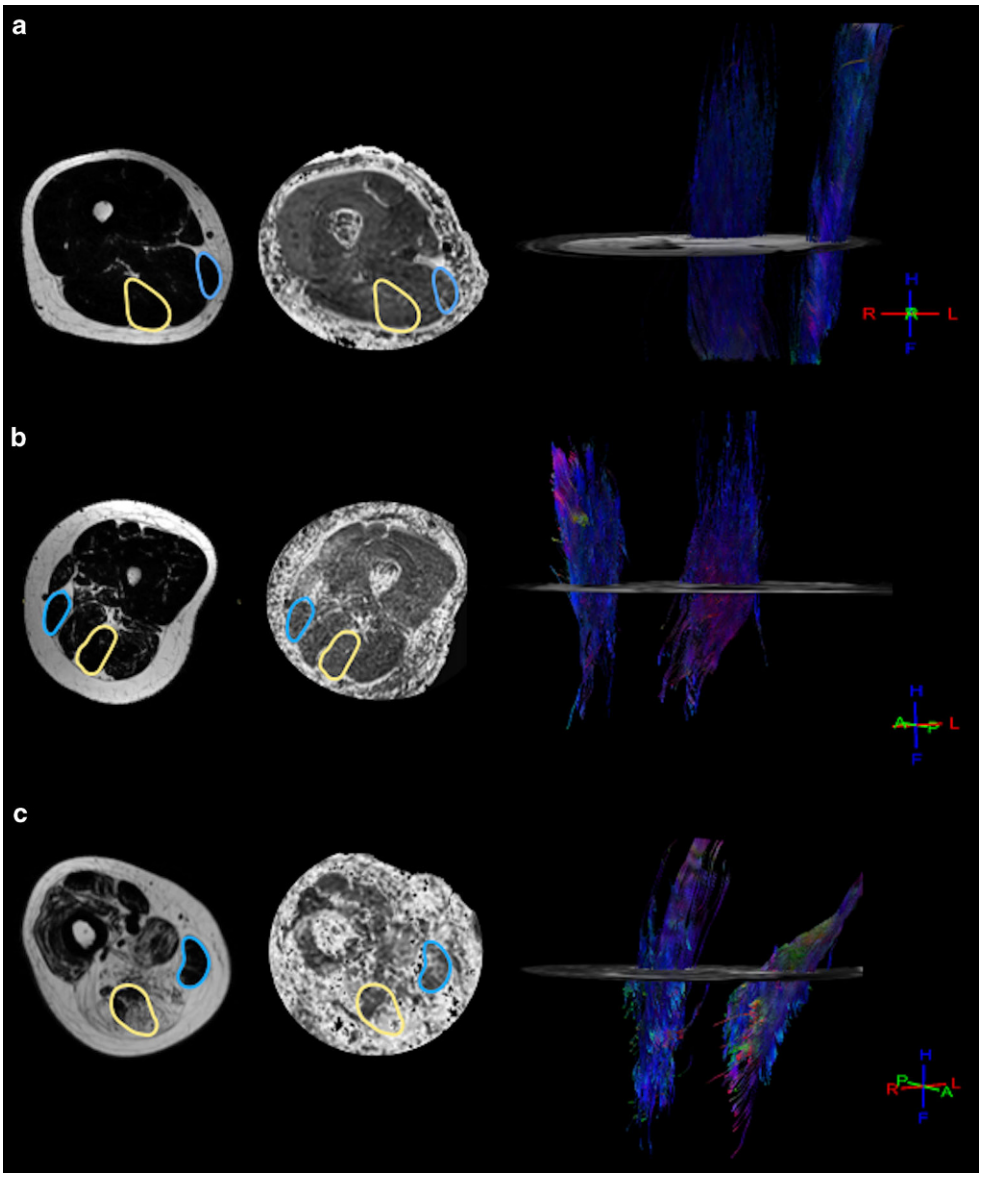

Fig. 4 Illustration of acquired images in controls and cases. *Left to right:* axial GRE fat only axial image (*yellow circle:* semitendinosus muscle, *blue circle:* gracilis muscle), axial grey scale FA map, and 3D tractography of selected muscles, **a** 32-year-old healthy female control. Gracilis muscle MFF 3.5%, semitendinosus muscle MFF 3.0% with dense distribution of tracts within the selected muscle bundles, **b** 34-year-old male case diagnosed Becker muscular dystrophy with mild fatty infiltration of the semitendinosus muscle (MFF 5.7%) and gracilis muscle (G 5.0%), **c** 31-year-old male case diagnosed Becker muscular dystrophy with moderate to severe fatty replacement of the semitendinosus muscle (MFF 47.8%) and gracilis muscle (MFF 22.2%) (*A* anterior, *P* posterior, *H* head, *F* feet, *R* right, *L* left)

ization, but that ROI localization significantly reduced the negative effect of MFF on FTL (Table 5; Fig. 6).

Discussion

The results of our study show the differences in quantitative DTI parameters of skeletal muscle with varying degrees of fatty replacement due to dystrophic processes. The heterogeneous distribution of fat replacement was used to apply two variants of ROI segmentation, a custom whole muscle ROI and a selective ROI, excluding areas of gross muscular fat.

A strong and consistent association of DTI metrics and FTL with MFF on custom ROI segmentation was confirmed by correlation analysis of this study. This association is in line with previous literature from Li et al. [31] and Ponrartana et al. [9] who found significant associations of FA and ADC with muscle fat in patients diagnosed with Duchenne muscular dystrophy. By applying a muscle-selective ROI in cases, the association of MFF and DTI metrics was reduced, but still significant on correlation analysis in ST, BF and G muscle. This finding is consistent with results of the interaction analysis where no significant effect of selective ROI segmentation on the association of MFF on ADC and FA was identified. The influence of fatty replacement on DTI metrics has been analyzed in previous studies. Williams et al. [16] reported an artificial increase of FA and artificial decrease of ADC in the setting of high fat content (>45% fat signal). Furthermore, Williams et al. supposed that the increase of FA could be partially related to error from random noise because of the signal loss from using

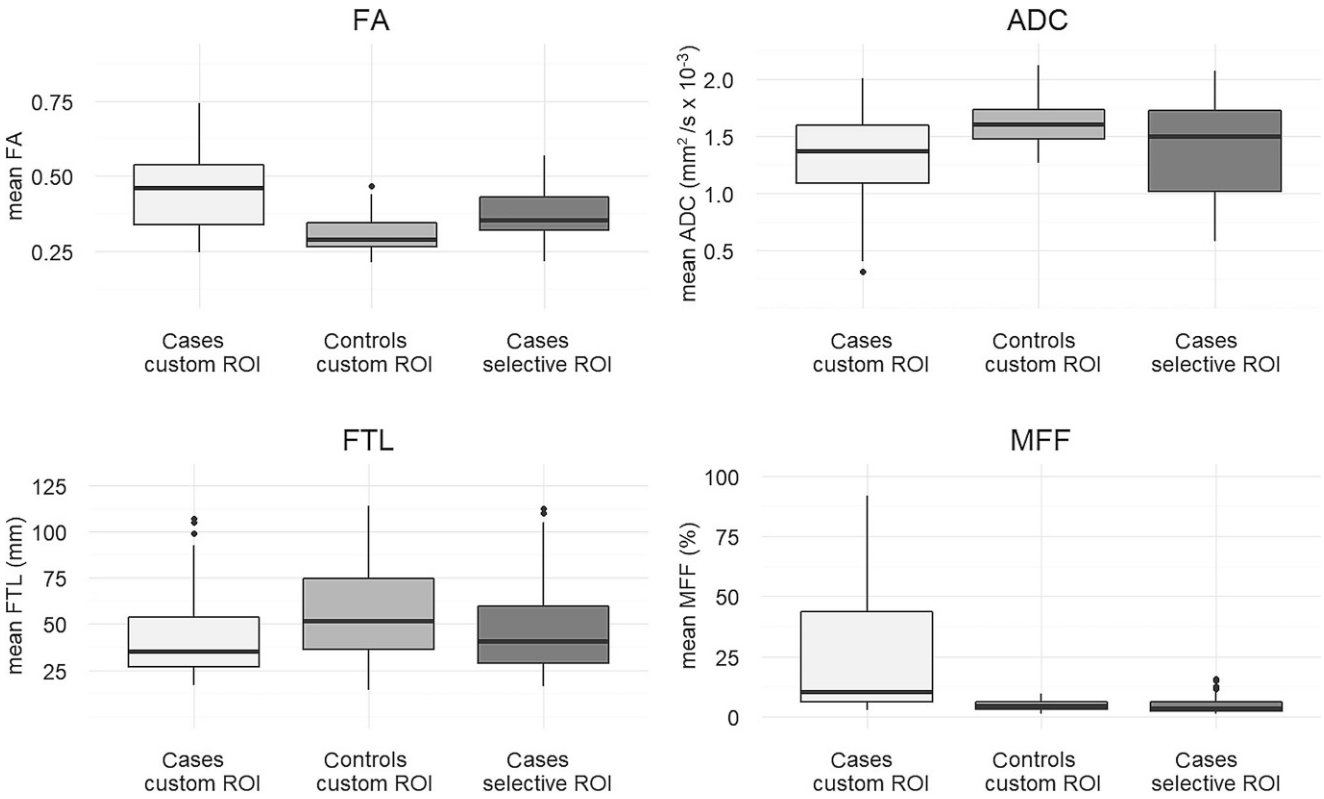

Fig. 5 Boxplots of DTI metrics, FTL, and MFF in controls and in cases custom and selective ROI. Center line shows the medians, boxplot limits the 25th–75th percentiles. Whiskers extend to the maximum observed value within 1.5 times the interquartile range from the 25th and the 75th percentile. Outliers are drawn as individual points. Significant differences are observed between custom ROI cases and controls (ADC, FA, FTL, MFF: $P < 0.001$), and between custom and selective ROI FA and MFF in cases ($P < 0.001$), but not ADC ($P = 0.49$) and FTL ($P = 0.59$)

a fat-suppressed echo planar imaging sequence on predominantly fat replaced tissue. These effects can be understood in simple terms by using extreme examples. For example, when FA is low, the three diffusion eigenvalues are approximately the same. Noise will cause fluctuations in the three measured diffusion eigenvalues to make them more different, leading to an FA increase [32]. Furthermore, noise will make the measured diffusion-weighted signal larger than the true signal when the true signal is small, and an overestimation of diffusion-weighted MR signal translates into underestimation of diffusion coefficients. The fat infiltration in patients decreases the muscle partial volumes in image voxels and decreases the SNR. As can be seen in Fig. 5, FA is increased and ADC is decreased in cases, especially in values from custom ROI. By excluding high fat areas in the selective ROI, we expect the bias in FA and ADC measurements to decrease; we applied an interaction analysis based on mixed model effects to corroborate or discard this hypothesis.

The finding that exclusion of gross muscular fat by applying the selective ROI segmentation has no effect on the association of MFF on ADC and FA, also reinforces previous studies which stated that changes in tensor metrics are not only an expression of fat signal, but also that the structural derangement of muscle fibers itself should be considered when interpreting these tensor metrics in muscular dystrophy [9]. Structural changes can be visualized and quantified by using 3D tractography and measurement of FTL. For FTL a significant association with MFF was only observed on custom analysis, but this association was mitigated in major parts by applying the selective ROI segmentation. As opposed to ADC and FA, the association of MFF and FTL was significantly reduced by selective ROI segmentation. The mechanism behind the observed shortening of FTL in dystrophic muscle can be explained as follows: the shortening of the fiber under the applied technical algorithms in cases with higher percentage of MFF is probably influenced by the fact that DTI is fat-suppressed, leading to higher noise in voxels of areas with fatty infiltration, resulting in a random principal diffusion direction (e. g. large jumps in measured fiber direction from voxel to voxel), and therefore preterm termination of fiber tracking. By applying the FACT method [22, 23], ADC and FA are automatically measured along the reconstructed fiber track and not the FA map. Our applied thresholds on the fiber tracking algorithm (FA < 0.1; direction threshold >27°; minimum FTL 10 mm) are supposed to block the reconstruction of tracks from random noise; however, as seen in our data of custom

Table 4 Pearson correlation coefficients[a] of custom and selective ROI localization DTI metrics and FTL with MFF by muscle

Muscle ID		Pearson correlation coefficient with % muscle fat fraction (95% CI)		
Cases				
–	Region of interest (ROI)	FA	ADC	FTL
RF	Custom	**0.83 (0.55; 0.94)**	**–0.85 (–0.95; –0.61)**	–0.31 (–0.71; 0.24)
	Selective	0.21 (–0.39; 0.68)	–0.34 (–0.75; 0.26)	–0.05 (–0.58; 0.52)
ST	Custom	**0.93 (0.8; 0.98)**	**–0.89 (–0.96; –0.69)**	**–0.83 (–0.94; –0.54)**
	Selective	**0.72 (0.27; 0.91)**	**–0.76 (–0.92; –0.36)**	**–0.58 (–0.86; –0.04)**
G	Custom	**0.86 (0.62; 0.95)**	**–0.91 (–0.97; –0.75)**	**–0.51 (–0.81; –0.00)**
	Selective	**0.57 (0.03; 0.85)**	**–0.65 (–0.88; –0.15)**	–0.32 (–0.74; 0.28)
BF	Custom	**0.91 (0.74; 0.97)**	**–0.89 (–0.96; –0.69)**	**–0.68 (–0.88; –0.25)**
	Selective	**0.69 (0.23; 0.9)**	**–0.73 (–0.91; –0.31)**	–0.33 (–0.75; 0.27)
Controls				
RF		–0.21 (–0.72; 0.45)	–0.25 (–0.74; 0.41)	0.34 (–0.32; 0.78)
ST		–0.50 (–0.14; 0.85)	–0.31 (–0.77; 0.35)	0.25 (–0.41; 0.74)
G		–0.37 (–0.79; 0.29)	–0.45 (–0.83; 0.20)	0.10 (–0.53; 0.66)
BF		–0.21 (–0.72; 0.45)	–0.01 (–0.61; 0.59)	0.39 (–0.27; 0.80)

Bold print Significant correlation ($P < 0.05$)
Custom ROI cases, $N = 15$ per muscle
Custom ROI controls, $N = 11$ per muscle
Selective ROI cases, $N = 13$ per muscle
FA fractional anisotropy, *ADC* apparent diffusion coefficient, *FTL* fiber track length, *RF* rectus femoris muscle, *ST* semitendinosus muscle, *G* gracilis muscle, *BF* biceps femoris muscle, *CI* confidence interval
[a]Based on mixed effects models with random intercepts for person

Table 5 Interaction analysis[a] of the association of MFF with DTI metrics and FTL depending on ROI localization in cases

Dependent variable	Independent variables	Estimate (95% CI)
FA	Intercept	**0.335 (0.270; 0.399)**
	MFF	**0.008 (0.002; 0.014)**
	Custom ROI	0.031 (–0.003; 0.065)
	Interaction: MFF[a] custom ROI	–0.005 (–0.010; 0.001)
ADC	Intercept	**1.523 (1.217; 1.832)**
	MFF	**–0.024 (–0.045; –0.004)**
	Custom ROI	0.079 (–0.049; 0.205)
	Interaction: MFF[a] custom ROI	0.012 (–0.007; 0.032)
FTL	Intercept	**58.152 (44.605; 71.784)**
	MFF	**–2.081 (–3.654; –0.502)**
	Custom ROI	–2.133 (–13.263; 8.735)
	Interaction: MFF[a] custom ROI	**1.617 (0.058; 3.182)**

Bold print Significant regression coefficient ($P < 0.05$)
MFF muscle fat fraction, *FA* fractional anisotropy, *ADC* apparent diffusion coefficient, *FTL* fiber track length, *ROI* region of interest
[a]Based on mixed effects models with random intercepts for muscle and person ($N = 112$)

ROI segmentation, where areas of gross muscular fat are included into the region-of-interest, a few measurements of presumed noise evade these thresholds and are inadvertently included in ADC and FA measurements. One method to circumvent this bias could be to increase the threshold of FTL, however, by doing so, there is also a risk of excluding dystrophic and deranged real fibers from analysis, which would then artificially normalize derived tensor metrics.

A major limitation of DTI on dystrophic muscle is that no algorithm exists so far to quantify the contribution of noise on tensor metrics, and therefore, the proportion of pathophysiological changes on FA and ADC can only be estimated. The application of selective ROI segmentation mitigates the influence of fat-induced random noise, but before suggesting this method as a potential biomarker in muscular dystrophy, further studies on DTI metrics and histopathological correlation are needed.

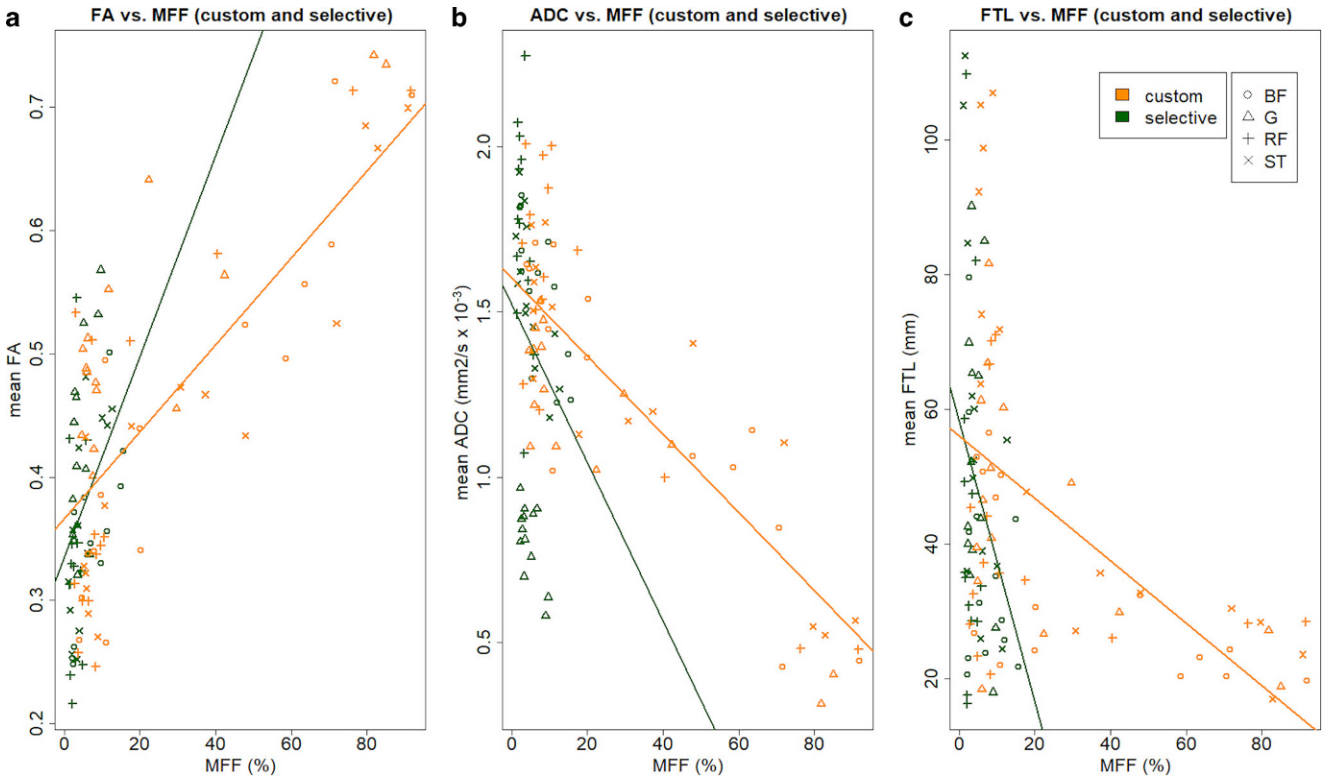

Fig. 6 Effect of custom ($N = 60$) and selective ROI ($N = 52$) segmentation on association of MFF with DTI metrics and FTL in cases (based on mixed effects models with random intercepts for muscle and person)

Another limitation is the small number of cases ($N = 15$) in our study but mitigated by the fact of several measurements per person. The small prevalence of dystrophic muscle diseases (1–5: 100,000 [33, 34]) depending on the subtype, rendered the recruitment of cases difficult and resulted in heterogeneity of the study cohort. Furthermore, based on recent studies showing negligible T2 effects on tensor metrics [14, 15] and also the inability of patients to endure long scanning times, we refrained from obtaining simultaneous T2 mapping in our study. Furthermore, the visual assessment of muscle edema on T2w mDixon images revealed endomysial edema only in vastus and adductor muscle groups (Table 1), which were not included in quantitative analysis.

Conclusion

Diffusion tensor imaging and chemical-shift-encoded water-fat MRI provide non-invasive insights on muscle fiber architecture in physiological and dystrophic conditions. A significant association of muscle fat and DTI metrics is observed in most dystrophic muscles of cases, but not controls. This association is weakened by applying a selective ROI segmentation, but not significantly influenced by ROI localization using interaction analysis; however, for FTL, ROI localization significantly reduces the effect of MFF, suggesting that this method could be the better option for MR tractography.

Acknowledgements We kindly thank Dr. Jan Sedlacik (Department of Neuroradiology, University Medical Center Hamburg-Eppendorf) for the critical review of this work.

Conflict of interest S. Keller, Z.J. Wang, A. Aigner, A.C. Kim, A. Golsari, G. Adam and J. Yamamura declare that they have no competing interests. H. Kooijman is an employee of Philips Healthcare.

References

1. Ward SR, Winters TM, Blemker SS. The architectural design of the gluteal muscle group: implications for movement and rehabilitation. J Orthop Sports Phys Ther. 2010;40:95–102.
2. Bodine SC, Roy RR, Meadows DA, Zernicke RF, Sacks RD, Fournier M, Edgerton VR. Architectural, histochemical, and contractile characteristics of a unique biarticular muscle: the cat semitendinosus. J Neurophysiol. 1982;48:192–201.
3. Burkholder TJ, Fingado B, Baron S, Lieber RL. Relationship between muscle fiber types and sizes and muscle architectural properties in the mouse hindlimb. J Morphol. 1994;221:177–90.
4. Oudeman J, Nederveen AJ, Strijkers GJ, Maas M, Luijten PR, Froeling M. Techniques and applications of skeletal muscle diffusion tensor imaging: a review. J Magn Reson Imaging. 2016;43:773–88.
5. Ahmad CS, Redler LH, Ciccotti MG, Maffulli N, Longo UG, Bradley J. Evaluation and management of hamstring injuries. Am J Sports Med. 2013;41:2933–47.

6. Basser PJ, Jones DK. Diffusion-tensor MRI: theory, experimental design and data analysis—a technical review. NMR Biomed. 2002;15:456–67.
7. Galbán CJ, Maderwald S, Stock F, Ladd ME. Age-related changes in skeletal muscle as detected by diffusion tensor magnetic resonance imaging. J Gerontol A Biol Sci Med Sci. 2007;62:453–8.
8. Galbán CJ, Maderwald S, Uffmann K, Ladd ME. A diffusion tensor imaging analysis of gender differences in water diffusivity within human skeletal muscle. NMR Biomed. 2005;18:489–98.
9. Ponrartana S, Ramos-Platt L, Wren TA, Hu HH, Perkins TG, Chia JM, Gilsanz V. Effectiveness of diffusion tensor imaging in assessing disease severity in Duchenne muscular dystrophy: preliminary study. Pediatr Radiol. 2015;45:582–9.
10. Saotome T, Sekino M, Eto F, Ueno S. Evaluation of diffusional anisotropy and microscopic structure in skeletal muscles using magnetic resonance. Magn Reson Imaging. 2006;24:19–25.
11. Sinha S, Sinha U, Edgerton VR. In vivo diffusion tensor imaging of the human calf muscle. J Magn Reson Imaging. 2006;24:182–90.
12. Damon BM, Ding Z, Anderson AW, Freyer AS, Gore JC. Validation of diffusion tensor MRI-based muscle fiber tracking. Magn Reson Med. 2002;48:97–104.
13. Mori S, van Zijl PC. Fiber tracking: principles and strategies—a technical review. NMR Biomed. 2002;15:468–80.
14. Froeling M, Nederveen AJ, Nicolay K, Strijkers GJ. DTI of human skeletal muscle: the effects of diffusion encoding parameters, signal-to-noise ratio and T2 on tensor indices and fiber tracts. NMR Biomed. 2013;26:1339–52.
15. Hooijmans MT, Damon BM, Froeling M, Versluis MJ, Burakiewicz J, Verschuuren JJ, Niks EH, Webb AG, Kan HE. Evaluation of skeletal muscle DTI in patients with duchenne muscular dystrophy. NMR Biomed. 2015;28:1589–97.
16. Williams SE, Heemskerk AM, Welch EB, Li K, Damon BM, Park JH. Quantitative effects of inclusion of fat on muscle diffusion tensor MRI measurements. J Magn Reson Imaging. 2013;38:1292–7.
17. Gaeta M, Scribano E, Mileto A, Mazziotti S, Rodolico C, Toscano A, Settineri N, Ascenti G, Blandino A. Muscle fat fraction in neuromuscular disorders: dual-echo dual-flip-angle spoiled gradient-recalled MR imaging technique for quantification—a feasibility study. Radiology. 2011;259:487–94.
18. Dixon WT. Simple proton spectroscopic imaging. Radiology. 1984;153:189–94.
19. Hooijmans MT, Niks EH, Burakiewicz J, Anastasopoulos C, van den Berg SI, van Zwet E, Webb AG, Verschuuren JJGM, Kan HE. Non-uniform muscle fat replacement along the proximodistal axis in Duchenne muscular dystrophy. Neuromuscul Disord. 2017;27:458–64.
20. Díaz-Manera J, Llauger J, Gallardo E, Illa I. Muscle MRI in muscular dystrophies. Acta Myol. 2015;34:95–108.
21. Eggers H, Brendel B, Duijndam A, Herigault G. Dual-echo Dixon imaging with flexible choice of echo times. Magn Reson Med. 2011;65:96–107.
22. Mori S, Crain BJ, Chacko VP, van Zijl PC. Three-dimensional tracking of axonal projections in the brain by magnetic resonance imaging. Ann Neurol. 1999;45:265–9.
23. Mori S, Kaufmann WE, Davatzikos C, Stieltjes B, Amodei L, Fredericksen K, Pearlson GD, Melhem ER, Solaiyappan M, Raymond GV, Moser HW, van Zijl PC. Imaging cortical association tracts in the human brain using diffusion-tensor-based axonal tracking. Magn Reson Med. 2002;47:215–23.
24. Ma J. Dixon techniques for water and fat imaging. J Magn Reson Imaging. 2008;28:543–58.
25. R Development Core Team. A language and environment for statistical computing. Vienna: R Foundation for Statistical Computing; 2016.
26. Gamer M, Lemon J, Fellows I, Singh P. irr: various coefficients of interrater reliability and agreement. R package version 0.84. 16.07.2012 http://CRAN.R-project.org/package=irr. Accessed: 16.07.2012
27. Bates D, Mächler M, Bolker B, Walker S. Fitting linear mixed-effects models using lme4. J Stat Softw. 2015;67:1–48.
28. Chan WP, Liu GC. MR imaging of primary skeletal muscle diseases in children. AJR Am J Roentgenol. 2002;179:989–97.
29. Janssen BH, Voet NB, Nabuurs CI, Kan HE, de Rooy JW, Geurts AC, Padberg GW, van Engelen BG, Heerschap A. Distinct disease phases in muscles of facioscapulohumeral dystrophy patients identified by MR detected fat infiltration. PLoS One. 2014;9:e85416.
30. Regula JU, Jestaedt L, Jende F, Bartsch A, Meinck HM, Weber MA. Clinical muscle testing compared with whole-body magnetic resonance imaging in facio-scapulo-humeral muscular dystrophy. Clin Neuroradiol. 2016;26:445–55.
31. Li GD, Liang YY, Xu P, Ling J, Chen YM. Diffusion-tensor imaging of thigh muscles in Duchenne muscular dystrophy: correlation of apparent diffusion coefficient and fractional anisotropy values with fatty infiltration. AJR Am J Roentgenol. 2016;206:867–70.
32. Pierpaoli C, Basser PJ. Toward a quantitative assessment of diffusion anisotropy. Magn Reson Med. 1996;36:893–906.
33. Urtasun M, Sáenz A, Roudaut C, Poza JJ, Urtizberea JA, Cobo AM, Richard I, García Bragado F, Leturcq F, Kaplan JC, Martí Massó JF, Beckmann JS, López de Munain A. Limb-girdle muscular dystrophy in Guipuzcoa (Basque country, Spain). Brain. 1998;121(Pt 9):1735–47.
34. Mah JK, Korngut L, Dykeman J, Day L, Pringsheim T, Jette N. A systematic review and meta-analysis on the epidemiology of Duchenne and Becker muscular dystrophy. Neuromuscul Disord. 2014;24:482–91.

Affiliation

S. Keller[1] · Z. J. Wang[2] · A. Aigner[3] · A. C. Kim[4] · A. Golsari[5] · H. Kooijman[6] · G. Adam[1] · J. Yamamura[1]

Z. J. Wang
jerry.wang@childrens.com

A. Aigner
a.aigner@uke.de

A. C. Kim
Anne.C.Kim@kp.org

A. Golsari
agolsari@uke.de

H. Kooijman
hendrik.kooijman@philips.com

G. Adam
g.adam@uke.de

J. Yamamura
j.yamamura@uke.de

1 Department of Diagnostic and Interventional Radiology and Nuclear Medicine, University Medical Center Hamburg-Eppendorf (UKE), Hamburg, Germany

2 Childrens' Medical Center Dallas, Department of Radiology, University of Texas Southwestern Medical Center, Dallas, TX, USA

3 Institute of Medical Biometry and Epidemiology, University Medical Center Hamburg-Eppendorf (UKE), Hamburg, Germany

4 Department Stroke and Neurovascular Imaging, The Permanente Medical Group, San Francisco, CA, USA

5 Department of Neurology, University Medical Center Hamburg-Eppendorf (UKE), Hamburg, Germany

6 Philips Healthcare, Hamburg, Germany